Available online at www.sciencedirect.com
ScienceDirect
Applied Mathematical Modelling 31 (2007) 1970–1996
APPLIED MATHEMATICAL MODELLING
www.elsevier.com/locate/apm

A 3D modeling of static and forward smoldering combustion in a packed bed of materials

M.S. Saidi [a], M.R. Hajaligol [b,*], A. Mhaisekar [b], M. Subbiah [b]

[a] *Saidi Partnership, Richmond, VA, United States*
[b] *Philip Morris USA, Research Center, Richmond, VA, United States*

Received 1 December 2005; received in revised form 1 April 2006; accepted 31 August 2006
Available online 27 October 2006

Abstract

A three-dimensional (3D) model based on the first principles of mass, momentum and energy was developed that numerically simulates the processes of static and forward smoldering in a porous packed bed of plant materials. The packed bed contains cellulose material or tobacco (cigarette) wrapped in a porous paper and surrounded by an ambient air. Other major characteristics of the model are including the effects of buoyancy forces in the flow field, separate treatment of solid and gas in a thermally non-equilibrium environment, and use of multi-precursor kinetic models for the pyrolysis of staring material and oxidation of char. The changes in porosity due to pyrolysis and char oxidation and the effect of porosity on the bed permeability and gas diffusivity are included. The mass, momentum, energy, and species transport equations are solved in a discretized computational domain using a commercially available computational fluid dynamics (CFD) code. The simulation results show that the model reasonably reproduces the major features of a burning cigarette during smoldering and puffing and are in a good agreement with the existing experimental results for cigarettes. Results include the velocity profiles, gas and solid temperatures, coal shape, burn rates, profile and transport of gas and vapor species throughout the packed bed, dilution through the wrapper paper and ventilation in the filter section, and the mass fraction of some pyrolysis and oxidation products in the mainstream and sidestream flows.

Keywords: Modeling; Smoldering; Combustion; Pyrolysis; Smoke; Heat and mass transfer

1. Introduction

Numerous modeling studies on pyrolysis and combustion of natural plant materials such as wood, cellulose and tobacco, that can sustain smoldering, have been reported in literature. Bruch et al. [1] numerically simulated the thermal decomposition of spherical wood particles of different sizes and varying properties by combining various processes such as heating, drying, pyrolysis, gasification, and combustion. Chan et al. [2]

* Corresponding author. Tel.: +1 804 274 2419; fax: +1 804 274 2891.
E-mail address: mohammad.r.hajaligol@pmusa.com (M.R. Hajaligol).

0307-904X/$ - see front matter
doi:10.1016/j.apm.2006.08.003

Nomenclature

A_i (s^{-1}) pre-exponent factor of the ith precursor of biomass pyrolysis; pre-exponent factor of the ith precursor of char oxidation
A_v (m^{-1}) surface to volume ratio of biomass column
A_w (s^{-1}) pre-exponent factor of moisture evaporation
A_{vr} (m^{-1}) surface to volume ratio of for coal radiation cooling
A_{ash} (m^{-1}) surface to volume ratio of coal ash
C_{pg} (kJ/kg K) gas average specific heat
C_{ps} (kJ/kg K) biomass shred specific heat
D_p (m) biomass column equivalent spherical particle average diameter
d_p (m) biomass column average pore size
D_{mm} (m^2/s) mass diffusion coefficient for a single component gas
D_t^d (m^2/s) thermal dispersion coefficient
D_m^d (m^2/s) mass dispersion coefficient
D_{AB} (m^2/s) mass diffusion coefficient of a binary gas mixture in a porous media
d_{AB} (m^2/s) mass diffusion coefficient of a binary gas mixture
E_{0i} (kJ/mol K) activation energy of the ith precursor of biomass pyrolysis; activation energy of the ith precursor of char oxidation
E_w (kJ/mol K) activation energy of moisture evaporation
f_{rad} coal radiation cooling position factor
h (W/m^2 K) biomass shreds–gas heat transfer coefficient
h_m (W/m^2 K) biomass shreds–gas mass transfer coefficient
$H_{combustion}$ (J/kg) char oxidation heat production rate
$H_{pyrolysis}$ (J/kg) biomass pyrolysis heat consumption rate
$H_{evaporation}$ (J/kg) biomass moisture evaporation heat consumption rate
$\dot{H}_{lighter}$ (W/m^3) lighter heat production rate
K_i (s^{-1}) kinetic constant of the ith precursor of biomass pyrolysis
K_{we} (s^{-1}) kinetic constant of the moisture evaporation
k_g (W/mK) gas thermal conductivity
k_s (W/mK) biomass shred thermal conductivity
$k_{s\,eff}$ (W/mK) biomass column solid phase effective thermal conductivity
$k_{g\,eff}$ (W/mK) biomass column gas phase effective thermal conductivity
k_r (W/mK) biomass column effective radiation conductivity
K (m^2) biomass column permeability
$Nu = \frac{hD_p}{k_g}$ Nusselt number
P (Pa) pressure
$Pr = v_g/\alpha_g$ Prandtl number
$Re = \frac{\bar{u}D_p}{v_g}$ Reynolds number
$Sh = \frac{h_m D_p}{\alpha_m}$ Sherwood number
$Sc = \frac{v_g}{\alpha_m}$ Schmidt number
T_g (K) gas temperature
T_s (K) solid temperature
T_∞ (K) ambient temperature
T_p (s) sinusoidal puff period
$\vec{V}$ (m/s) superficial velocity
V_i^* maximum yield if the ith precursor of biomass pyrolysis
V_i^n yield if the ith precursor of biomass pyrolysis at time t_n
V_{ci} yield if the ith precursor of char oxidation

V_{max} (m/s) maximum velocity of the sinusoidal puff profile
V_{puff} (m^3) puff volume
V_g (m^3) biomass column gas phase volume
V_s (m^3) biomass column solid phase volume
Y_i mass fraction of the smoke ith component
$Y^n_{o_2}$ mass fraction of oxygen at time t_n

Greek symbols
ρ_g (m^3/s) gas density
ρ_s (m^3/s) biomass shred density
ρ_{we} (m^3/s) biomass shred moisture density
ρ_{daf} (m^3/s) biomass shred dry-ash-free density
$\rho_{char,k}$ (m^3/s) kinetic controlled char oxidation density
$\rho_{char,m}$ (m^3/s) mass transfer controlled char oxidation density
ρ_{char} (m^3/s) char density
ρ_{py} (m^3/s) biomass pyrolysis density
ρ_{co} (m^3/s) CO density due to char oxidation
ρ_{co_2} (m^3/s) CO_2 density due to char oxidation
ρ_{o_2} (m^3/s) oxygen density
ρ_{ci} (m^3/s) the smoke ith component density
ρ_{ash} (m^3/s) ash density
ρ_b (m^3/s) porous media density
ν_g (m^2/s) gas kinematics viscosity
α_g (m^2/s) gas thermal diffusivity
α_m (m^2/s) gas mass diffusivity
μ (kg/ms) gas dynamic viscosity
τ porous media tortuosity
σ ($W/m^2\,K^4$) Stefan–Boltzmann constant
σ_i standard deviation of the ith precursor of biomass pyrolysis
ε emmisivity
ϕ biomass column porosity

presented a one-dimensional model of wood pyrolysis with inclusion of moisture release, tar cracking and char decomposition processes. A detailed mathematical model was developed by Miller et al. [3] to study the temporal and spatial solid–fluid reactions in spherically symmetric porous cellulose and wood particles. Bilbao et al. [4] presented a one-dimensional model to study the influence of moisture content on thermal decomposition of wood slabs. Drying and pyrolysis processes of large wood particles were modeled in one-dimension by Peters et al. [5] to predict transient thermal decomposition. Leach et al. [6] presented a one-dimensional transient model for forward smoldering allowing local thermal and chemical non-equilibrium. Fatehi et al. [7] modeled the adiabatic reverse combustion in packed bed of wood particles, allowing local thermal and chemical non-equilibrium between the phases. This one-dimensional model was used to describe the propagation of the reaction front through the fuel bed.

In this paper the main interest is in pyrolysis, combustion, and heat propagation in a media filled with shredded plant and natural materials. A large number of the works on shredded biomass materials are concentrated on cigarettes. Most of the available experimental data on smoldering combustion of shredded beds is also focused on cigarette burning. Therefore, the mathematical model, discussed in this paper, is primarily applicable to a cigarette type geometry filled with either tobacco or cellulose (paper) shreds. However, the model can be readily extended to other packed bed materials by including relevant geometry and applying appropriate boundary conditions.

Modeling the smoldering of a cigarette dates back to as early as 1960s by Egerton et al. [8]. They studied the physical mechanism of cigarette smoldering to elucidate the dependence of temperatures, consumption rates, etc., on cigarette structure and smoldering parameters. During 1980s, Ohlemiller [9] reviewed in detail different processes and mechanisms involved in smoldering process in general and specifically the burning of a cigarette. The mathematical models found in literature are limited to one and two-dimensional geometries. Among the one-dimensional mathematical models, one may refer to the works of Summerfield et al. [10] on modeling steady-draw smoking, Norbury and Stuart [11] on a transport model for porous medium combustion, Kansa [12] for modeling charring pyrolysis, including porous and permeable structures, Muramatsu et al. [13] for modeling natural smoldering of a cigarette, and Sandusky et al. [14] for modeling the forced smoldering (puffing) of a cigarette. The prominent two-dimensional models are the modeling of combustion processes of charring and non-charring solid fuels of slab geometry by Di Blasi [15], and a steady state model of a smoldering cylindrical geometry by Yi et al. [16]. Rostami et al. presented a transient model based on first principles for both natural [17] and forward smoldering [18] of a cigarette which considers the smoldering domain to have two independent phases of solid and surrounding gas interacting at the interfaces. Finally, Saidi et al. presented an experimental and numerical analysis of puff hydrodynamics [19] and also developed a 3D model to numerically simulate a burning cigarette during puffing [20], based on available temperature distribution inside the cigarette coal.

To the best of our knowledge, no one has reported a model of a burning cigarette that simulates both puffing and smoldering based on first principles. Therefore, in this work, we present a model of cigarette puffing and smoldering and then apply the model on a shredded cellulose bed. Modeling the process of puffing a cigarette involves the mechanism of continuously transferring from transient forward smoldering to static smoldering and vice versa. The geometry is a packed bed of shredded tobacco leafs and modeling involves treatment of the whole bed rather than just a single fuel particle. Even though the cigarette is geometrically symmetric, due to the considerable effect of buoyancy forces, the problem is inherently three-dimensional.

Table 1
Thermo-physical and geometrical properties of the materials used in the study

A_v	A_{ash}	ϕ	ρ_s	ρ_b
Biomass column physical properties				
4570	1000	0.78	1090	240
Unburned biomass column	Burned biomass column	Unburned wrapper paper	Burned wrapper paper	Filter
Permeability (m^2)				
5.6×10^{-10}	10^5	4.89×10^{-15}	10^5	2.5×10^{-10}
α_m (air) (m^2/s)	α_m (paper) (m^2/s)	α_m (filter) (m^2/s)	C_{ps} (kJ/kg K)	k_s (W/mK)
Some thermo-physical properties				
2.1×10^{-5}	4.68×10^{-7}	2.7×10^{-7}	1.38	0.27
ρ_s	ρ_{daf}	ρ_{we}	ρ_{char}	ρ_{ash}
Cellulose shred compositional density (kg/m^3)				
1090	937.4	87.2	225.0	65.4
ρ_s	ρ_{daf}	ρ_{we}	ρ_{char}	ρ_{ash}
Tobacco shred compositional density (kg/m^3)				
1090	931.5	109	177	49.7

$H_{combustion}$ (J/kg)	$-H_{pyrolysis}$ (J/kg)	$-H_{evaporation}$ (J/kg)	$\dot{H}_{lighter}$
Rates of heat generation or consumption			
Cellulose (32)			
2.5×10^7	5.7×10^5	2.26×10^6	2.0×10^8
Tobacco (31)			
1.76×10^7	2.09×10^5	2.26×10^6	2.0×10^8

In a step-by-step approach, the mathematical model is applied to derive a correlation for the gas diffusion coefficient through paper. Then the model is extended to simulate the transport of gaseous species in an unlit cigarette. Finally, the model is applied to a puffing cigarette filled with tobacco or cellulose shreds.

2. Mathematical formulation

The mathematical model is based on solving the partial differential equations of conservations of mass, momentum, and energy for a system containing a conventional cigarette and its surrounding air. The packed bed of cigarette rod with shredded tobacco particles is modeled as a porous media, which presents a resistance to the flow inside. The conservation equations on a macroscopic scale are derived by application of a volume averaging technique to the fundamental microscopic transport equations in a porous media. The air–cigarette boundary is a part of the solution to be determined; an ambient boundary condition is applied on the far field boundary where the effect of the presence of the cigarette is negligible, and thus, imposes no pre-conditioning on the final solution. All the gases behave according to the ideal gas law. In order to reduce complexity we have omitted thermal swelling and/or shrinkage as the solid fuel undergoes pyrolysis and oxidation, and also have not considered volatile species condensation in this model.

2.1. Continuity equation

$$\frac{\partial(\phi\rho_g)}{\partial t} + \vec{\nabla}\cdot(\rho_g\vec{V}) = \mathrm{SOURCE}_{\mathrm{mass}}, \tag{1}$$

where $\mathrm{SOURCE}_{\mathrm{mass}}$ is equal to the net mass produced per unit volume per unit time due to moisture evaporation, tobacco pyrolysis and char oxidation:

$$\mathrm{SOURCE}_{\mathrm{mass}} = \frac{\mathrm{d}\rho_{\mathrm{vm}}}{\mathrm{d}t} + \frac{\mathrm{d}\rho_{\mathrm{we}}}{\mathrm{d}t} + \frac{\mathrm{d}\rho_{\mathrm{co_2}}}{\mathrm{d}t} + \frac{\mathrm{d}\rho_{\mathrm{co}}}{\mathrm{d}t} - \frac{\mathrm{d}\rho_{\mathrm{char}}}{\mathrm{d}t} - \frac{\mathrm{d}\rho_{\mathrm{o_2}}}{\mathrm{d}t}. \tag{2}$$

Table 2
Pyrolysis and char oxidation kinetic parameters of the biomass materials used in the study

Products	Kinetic parameters of cellulose pyrolysis [27]			
	A_i (s^{-1})	E_{0i}/R (K)	σ_i/R	Y_i (wt% daf)
CO_2	8.0×10^{11}	20,341	700	1.8
CO	8.0×10^{11}	20,341	700	0.75
H_2O	8.0×10^{11}	20,341	700	7.4
CH_4	8.0×10^{11}	38,000	4000	0.19
Tar	8.0×10^{11}	20,341	100	87.0
Formaldehyde	8.0×10^{11}	20,341	700	1.1
Formic acid	8.0×10^{11}	20,341	700	0.65
Acetic acid	8.0×10^{11}	20,341	700	0.4
	A_i (min^{-1})	E_{0i}/R (K)		V_{ci} (wt%)
Kinetic parameters for tobacco char oxidation [31]				
1	2.8×10^{6}	9813		50
2	1.15×10^{11}	19,123		50
	A_i (min^{-1})	E_{0i}/R (K)		Y_i (wt%)
Kinetic parameters for cellulose char oxidation [32]				
1	3.4×10^{11}	19,245		100
	A_i (s^{-1})	E_{0i}/R (K)		Y_i (wt%)
Kinetic parameters for biomass moisture evaporation [33]				
1	1.0×10^{12}	9813		100

2.2. Momentum equation

The general form of momentum equations for incompressible flow in a porous medium is given as [21]

$$\frac{\partial(\rho_g \vec{V})}{\partial t} + (\vec{V}\cdot\vec{\nabla})(\rho_g \vec{V}) = -\vec{\nabla}P + \vec{\nabla}\cdot(\mu\vec{\nabla})\vec{V} + \rho_g\vec{g} - \mathrm{SOURCE}_{\mathrm{momentum}}, \tag{3}$$

where $\vec{V}$ is the superficial velocity, the average local velocity, if there is no solid phase.

The source term $\mathrm{SOURCE}_{\mathrm{momentum}}$ represents the added pressure drop due to the presence of solid phase and is based on modified Ergun equation [22]:

$$\mathrm{SOURCE}_{\mathrm{momentum}} = \frac{\mu}{K}\vec{V} + \frac{F\rho_g}{K^{1/2}}|\vec{V}|\vec{V}. \tag{4}$$

In the above equation, the effect of inertia becomes important for $Re > 3$. For a packed bed of mono-sized spherical particles the permeability, K, is predicted by Carman–Kozeny model [23]:

$$K = \frac{\phi^3 D_p^2}{C_K(1-\phi)^2}, \tag{5}$$

where C_K is equal to 180 for spherical particles. However, for a packed bed of shredded material we expect the induced pressure drop to be higher and therefore C_K to be larger. The equivalent spherical particle diameter of the shredded bed is derived from the definition of bed porosity:

$$D_p = D_g\left(\frac{1-\phi}{\phi}\right)^{1/3}. \tag{6}$$

The tobacco column average pore diameter is $D_g = 4.4\times10^{-4}$ m [24]. Applying Eq. (6) for D_p and using Eq. (5) for C_K with a known permeability for the shredded bed as given in Table 1, we get values of 2.9×10^{-4} and 1300 for D_p and C_K, respectively.

2.3. Gaseous species transport equations

Having the velocity flow field, the gaseous species concentrations are determined by solving the gas transport equation in a porous media for each species [25]:

$$\frac{\partial(\rho_g\phi Y_i)}{\partial t} + (\vec{V}\cdot\vec{\nabla})(\rho_g Y_i) = \vec{\nabla}\cdot[\rho_g\phi(D_{gi} + D_m^d)\vec{\nabla}Y_i] + \mathrm{SOURCE}_i. \tag{7}$$

The source term SOURCE_i is the sum of the volumetric rate of production/consumption of gaseous species i due to evaporation, pyrolysis and char oxidation.

2.4. Energy equation

During the process of puffing, the time variation of the solid temperature is very rapid and the assumption of gas–solid thermal equilibrium is no longer valid. Therefore, a two-medium treatment is applied for the energy equation. The solid phase is treated as a continuum, and particle-scale gradients are excluded. The solid and gas phase energy equations [25] are

$$\frac{\partial((1-\phi)\rho_s c_{ps} T_s)}{\partial t} = \vec{\nabla}\cdot[(k_{seff} + k_r)\vec{\nabla}T_s] + hA_v(T_g - T_s) + \mathrm{SOURCE}_s, \tag{8}$$

$$\frac{\partial(\phi\rho_g C_{pg} T_g)}{\partial t} + \vec{\nabla}\cdot(\rho\vec{V}C_{pg}T_g) = \vec{\nabla}\cdot[(k_{geff} + \phi\rho_g C_{pg} D_t^d)\vec{\nabla}T_g] + hA_v(T_s - T_g), \tag{9}$$

respectively, where the source term SOURCE_s represents the sum of heat of char oxidation, pyrolysis, evaporation, radiation cooling and heat generated by the electric lighter:

$$\mathrm{SOURCE_s} = H_{\mathrm{combustion}}\frac{\mathrm{d}\rho_{\mathrm{c}}}{\mathrm{d}t} + H_{\mathrm{pyrolysis}}\frac{\mathrm{d}\rho_{\mathrm{py}}}{\mathrm{d}t} + H_{\mathrm{evaporation}}\frac{\mathrm{d}\rho_{\mathrm{w}}}{\mathrm{d}t} + \dot{H}_{\mathrm{lighter}} + \sigma\varepsilon A_{\mathrm{vr}} f_{\mathrm{rad}}(T_\infty^4 - T_{\mathrm{s}}^4). \tag{10}$$

The radiation heat exchange with the environment takes place on the coal surface and f_{rad} is set zero everywhere except in this region where it is set to one. The parameter A_{vr} is the computational cell surface to cell volume ratio and is equal to the cell surface area facing towards the environment divided by the cell volume and C_{pg} is the mass weighted average specific heat capacity of the gaseous species.

3. Mathematical sub-models

The above-mentioned conservation equations are supported by a number of sub-models that are described in the following sections:

3.1. Pyrolysis of shredded materials

We consider the shredded biomass to be made of either cellulose or tobacco leaf. Pyrolysis studies [26] have shown that the conditions can be chosen such that the decomposition is kinetically controlled, i.e., transport processes such as heat and mass transfer is much faster compared to the rate of chemical decomposition of the biomass. Assuming an Arsenics type equation for the pyrolysis reaction of shredded material, the rate of pyrolysis is calculated using the 7-precursor kinetic parameters [27] given in (Table 2) for cellulose and the 42-precursor kinetic parameters for tobacco provided by Wojtowicz et al. [28]. For a single species i, the reaction rate equation can be written as [29]

$$\frac{\mathrm{d}V_i}{\mathrm{d}t} = K_i(V_i^* - V_i); \quad K_i = \int_{-\infty}^{+\infty} A_i \exp(-E/RT_{\mathrm{s}}) \frac{\exp\left(-\frac{1}{2}\left(\frac{E-E_{0i}}{\sigma_i}\right)^2\right)}{\sigma_i\sqrt{2\pi}}\,\mathrm{d}E. \tag{11}$$

After some mathematical simplification, Eq. (11) reduces to

$$K_i = A_i \exp\left[-\frac{E_{0i}}{RT_{\mathrm{s}}}\left(1 - \frac{\alpha_i}{T_{\mathrm{s}}}\right)\right]; \quad \alpha_i = \frac{(\sigma_i/R)^2}{2(E_{0i}/R)}, \tag{12}$$

$$V_i^{n+1} = V_i^*(1 - (1 - V_i^n/V_i^*)\exp(-K_i\Delta t)); \quad \Delta t = t_{n+1} - t_n. \tag{13}$$

To gain a second order accuracy in the above calculations K_i is calculated based on new and old values of solid temperature. The volumetric rate of production of each component is calculated as

$$\frac{\Delta\rho_{\mathrm{py}}}{\Delta t} = \rho_{\mathrm{daf}} \sum_j \frac{(V_i^{n+1} - V_i^n)}{(t_{n+1} - t_n)}. \tag{14}$$

3.2. Char formation and oxidation

The rate of char production due to pyrolysis is calculated in terms of the total rate of tobacco pyrolyzed:

$$\frac{\Delta\rho_{\mathrm{cp}}}{\Delta t} = a_{\mathrm{c}}\frac{\Delta\rho_{\mathrm{py}}}{\Delta t}, \tag{15}$$

where $a_{\mathrm{c}} = 0.17$ for bright tobacco.

We consider the following reaction for char oxidation:

$$\mathrm{C} + n\mathrm{O_2} \rightarrow n_1\mathrm{CO} + n_2\mathrm{CO_2}. \tag{16}$$

The split between CO and CO_2 is a function of temperature and is derived as

$$R_{\mathrm{CO/CO_2}} = \frac{\mathrm{kg\,mol\,CO}}{\mathrm{kg\,mol\,CO_2}} = \frac{n_1}{n_2} = A_{\mathrm{cc}} \exp(E_{\mathrm{cc}}/RT), \tag{17}$$

where $A_{\mathrm{cc}} = 1.0$, $E_{\mathrm{cc}} = 0.2$ kcal/mol [30] and n_1 and n_2 are derived in terms of $R_{\mathrm{co/co_2}}$:

$$n_1 = \frac{R_{co/co_2}}{1 + R_{co/co_2}}; \quad n_2 = \frac{1}{1 + R_{co/co_2}}. \tag{18}$$

If char oxidation is only kinetic controlled, the Mauramatsu's two equation model [31] is applied to calculate the rate of tobacco char oxidation:

$$\frac{\Delta\rho_{char,k}}{\Delta t} = \rho^n_{char}\sqrt{Y^n_{o_2}}\sum_{i=1}^{2} V^*_{ci}(1 - \exp(-K_i\Delta t)). \tag{19}$$

In case of cellulose, a one equation model provided by Di Blasi [32] is used, and the parameters A_i, E_i, and V^*_{ci} are given in Table 2. On the other hand, if char oxidation is only mass transfer controlled, then the rate of char oxidation is controlled by the rate of oxygen transferred to the char. In this case, the oxygen concentration on the char surface can be assumed zero and thus

$$\frac{\Delta\rho_{char,m}}{\Delta t} = N^*_{o_2} Y^{n*}_{o_2}\rho^{n*}_g A^*_{vt} h^n_m / n_{mass}, \tag{20}$$

where the superscript refers to time step t_n. The overall rate of char oxidation is determined by the combination of the above-mentioned rates:

$$\frac{\Delta\rho_{char}}{\Delta t} = \left[\left(\frac{\Delta\rho_{char,k}}{\Delta t}\right)^{-1} + \left(\frac{\Delta\rho_{char,m}}{\Delta t}\right)^{-1}\right]^{-1}. \tag{21}$$

Due to the shreds pore resistance for oxygen diffusion through the pore, the rate of char oxidation is less than expected. In order to compensate for this additional resistance, a correction term (n_{mass}) is included in the equation. This parameter was determined by matching the numerical and experimental results. As shown later, if we set $n_{mass} = 2$ it leads to a good match between the numerical and experimental results. The net rate of char production is the difference between the rate of char produced by pyrolysis and the rate of char consumed by oxidation:

$$\frac{\Delta\rho_c}{\Delta t} = \frac{\Delta\rho_{cp}}{\Delta t} - \frac{\Delta\rho_{char}}{\Delta t}. \tag{22}$$

3.3. Moisture evaporation

The moisture evaporation is represented as a heterogeneous reaction between liquid water and water vapor [33]:

$$\frac{d\rho_{we}}{dt} = -K_{we}\rho_{we}; \quad K_{we} = A_{we}\exp(-E_{we}/RT), \tag{23}$$

where $A = 5.13 \times 10^6\ s^{-1}$ and $E = 24$ kJ/mol are global values for evaporation of water from wood particles which are empirically obtained assuming particles are small and transport processes such as heat transfer is not limiting the evaporation. We applied the same parameters for tobacco shred and neglected the effect of bound water.

3.4. Thermo-physical properties

3.4.1. Effective thermal conductivities

The most common method is based on the assumption of the volumetric effective conductivities of the solid medium, $(1 - \phi)k_s$ and the gas medium, ϕk_g [34]. However, the solid or gas phase effective thermal conductivities calculated based on volumetric averages does not take into account the dependency of the conductivity of each phase on the other. Cheng [35], based on the experimental data, derived the following correlation for the bed effective thermal conductivity:

$$k_{eff} = k_s(k_g/k_s)^{0.69}. \tag{24}$$

By combining the above two approaches, the effective thermal conductivity of each phase is calculated as

$$k_{\text{seff}} = k_{\text{eff}} \frac{(1-\phi)k_{\text{s}}}{\phi k_{\text{g}} + (1-\phi)k_{\text{s}}}, \tag{25}$$

$$k_{\text{geff}} = k_{\text{eff}} \frac{\phi k_{\text{g}}}{\phi k_{\text{g}} + (1-\phi)k_{\text{s}}}. \tag{26}$$

3.4.2. Dispersion coefficients

The simultaneous existence of temperature and velocity gradients within the pore causes spreading of heat, which is in addition to the Darcian convection and the effective (collective) molecular conduction. Due to volume averaging over the pore space, this contribution is not included in the Darcian convection, and because of its dependence on ∇T, it is added as a dispersion coefficient to the effective thermal conductivity [36]. Different models are proposed for determining dispersion coefficient [37–40]. Here, we apply the correlation proposed by Vortmeyer [38] which is close to the ones given by Koch and Brady [39] and, Edwards and Richardson [40]

$$D_{\text{t}}^{\text{d}} = 0.8\alpha_{\text{t}} RePr. \tag{27}$$

The mass dispersion coefficient, D_{m}, is calculated from an equation similar to the above equation:

$$D_{\text{m}}^{\text{d}} = 0.8\alpha_{\text{m}} ReSc. \tag{28}$$

3.4.3. Solid–gas heat and mass transfer coefficients

There have been two different approaches for treating the heat transfer problem in packed beds of spherical particles at low Peclet numbers. In one approach, the gas diffusivity is replaced by the sum of stagnant diffusivity and convective (dispersion) diffusivity in the gas energy and species transport equations [41,42], while in the other approach the effect of the above terms is lumped into an apparent Nusselt number [43,44]. In this work we follow the first approach and apply the Wakao correlation [45] for the Nusselt number of a packed bed of spherical particles:

$$Nu = 2 + 1.1 Re_{\text{d}}^{0.6} Pr^{0.33}. \tag{29}$$

In the above equation the stagnant flow limiting value is sensitive to particle geometry and is 2 for a bed of spherical particles while the flow dependent part is less sensitive [46]. Therefore, we assume that a bed of shredded bed follows the following correlation:

$$Nu_{\text{d}} = Nu_{0\text{b}} + 1.1 Re_{\text{d}}^{0.6} Pr^{0.33}. \tag{30}$$

The bed is made of shreds and each shred has slab type geometry. The stagnant flow Nusselt number for a plate of thickness D, width W, and length L is given as [47]

$$Nu_0 = Sh_0 = \pi/[(1 + W/D + W/L)\ln(4L/W)]. \tag{31}$$

The bed shreds have the same thickness and width but a different length. The average length is determined so that the average single shred has a solid–gas interfacial area equal to the bed corresponding value. Considering $D = 0.12$ mm and $W = 0.85$ mm, results in $L = 1.4$ mm and finally Eq. (31) leads to $Nu_0 = 0.19$. The characteristic length in Eqs. (30) and (31) are D_{p} and D, respectively. Replacing D with D_{p} results $Nu_0 = 0.45$. On the other hand, the Nusselt number of a single shred and a packed bed of shreds of porosity ϕ correlated as [46]

$$Nu_{0\text{b}} = (1 + 1.5(1-\phi))Nu_0 = 0.7. \tag{32}$$

Based on Reynolds analogy and since in the cases of our interest the Lewis number is close to one, similar correlations are valid for mass transfer coefficient:

$$Sh_d = Sh_{0b} + 1.1Re_d^{0.6}Sc^{0.33}; \quad Sh_{0b} = 0.7. \tag{33}$$

3.4.4. Radiation heat transfer

In the cigarette coal where the solid temperature is very high, e.g., 1200 K, the radiation heat transfer cannot be ignored. Assuming the gas participation in radiation heat transfer is negligible, the solid–solid radiative heat transfer is compensated by adding an equivalent term, k_r to the solid phase effective thermal conductivity in the solid energy equation [48]:

$$k_r = 4FD_p\sigma T_s^3, \tag{34}$$

where F is calculated from the following equation:

$$F = 0.1843 + 0.5756\tan^{-1}\left[\frac{1.535}{\varepsilon_r}\left(\frac{k_s}{4D_p\sigma T_s^3}\right)^{0.8011}\right]. \tag{35}$$

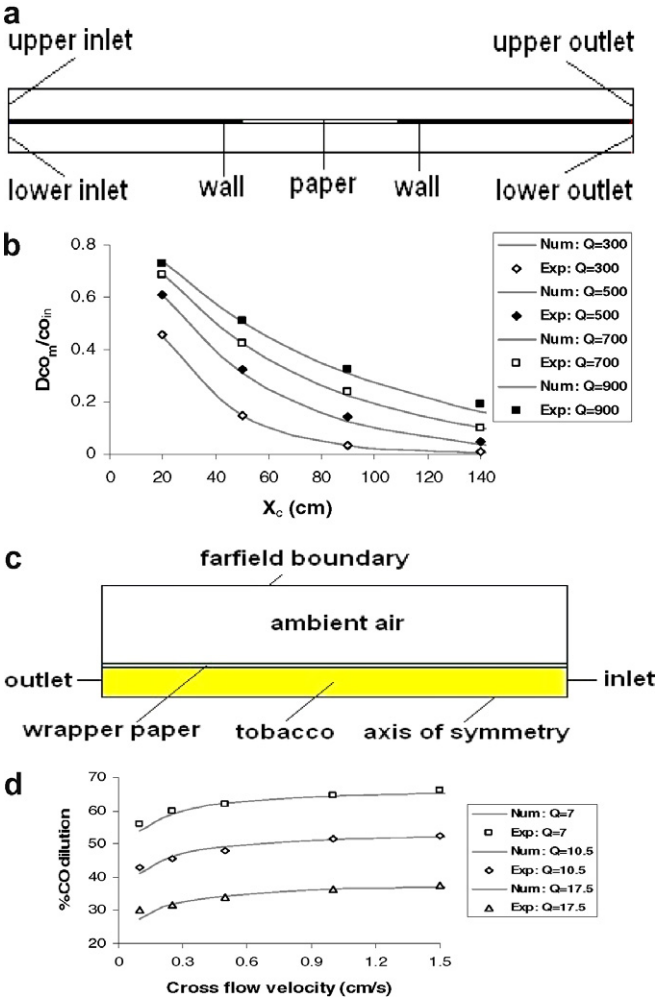

Fig. 1. Results of the experiments and simulation on paper: (a) schematic of the domain used in the experiment, (b) relative difference in CO mass fraction, (c) computational domain for the paper, and (d) total dilution of CO at different flow rates.

3.4.5. Gas viscosity

The effect of temperature on gas viscosity (μ) is implemented with Sutherland's two-coefficient law [49]:

$$\mu = \frac{C_1 T^{3/2}}{T + C_2}, \tag{36}$$

where $C_1 = 1.458 \times 10^{-6}$ kg/m s $K^{1/2}$ and $C_2 = 110.4$ K.

3.4.6. Gas diffusivity in shredded column

The gas diffusivity is a function of gas temperature and pressure. For a gas mixture the Fuller–Schettler–Giddings binary mixture model [50] is used for determining the mass diffusion coefficients:

$$d_{AB} = 0.0436 \frac{(T/273)^{1.75}}{P(V_A^{1/3} + V_B^{1/3})^2} \sqrt{1/M_A + 1/M_B}; \quad \mathrm{m}^2/\mathrm{s}, \tag{37}$$

where T and P are temperature and pressure, respectively; and, M_A, M_B, V_A and V_B are the molecular weights and molecular volumes of constituents A and B, respectively. For air at atmospheric pressure and 300 K, the diffusion coefficient of oxygen is 2.1×10^{-5} m^2/s. In the porous media the mass diffusivity decreases with bed porosity and its effect is considered as [49]

$$D_{AB} = d_{AB}\phi^{1.18}. \tag{38}$$

3.4.7. Physical properties

The physical properties of the tobacco column are depicted in Table 1. Given the shredded bed average density and the shred density, the bed initial porosity is calculated from the following equation which is based on the definition of porosity:

$$\phi = 1 - \rho_b/\rho_s. \tag{39}$$

The solid–gas interfacial area per unit volume based on equivalent spherical particle diameter is given as

$$A_V = 6(1 - \phi)/D_P. \tag{40}$$

As the cigarette burns, its permeability, porosity, and solid–gas interfacial area change. Also the tobacco column packing density changes during the burning process. This change in packing bed density is determined by calculating the mass lost due to moisture evaporation, pyrolysis, and char oxidation:

$$\frac{\mathrm{d}\rho_b}{\rho t} = -\frac{\Delta\rho_{py}}{\Delta t} - \frac{\Delta\rho_{char}}{\Delta t} - \frac{\Delta\rho_{we}}{\Delta t}. \tag{41}$$

The change in bed permeability, porosity, and solid–gas interfacial area is derived by assuming a linear correlation between bed density change and these above-mentioned parameters:

$$\phi = \phi_{ash} + (\phi_0 - \phi_{ash})\left(\frac{\rho_b - \rho_{ash}}{\rho_{0b} - \rho_{ash}}\right), \tag{42}$$

$$K = K_{ash} + (K_0 - K_{ash})\left(\frac{\rho_b - \rho_{ash}}{\rho_{0b} - \rho_{ash}}\right)^{-1}, \tag{43}$$

$$A_v = A_{ash} + (A_{0v} - A_{ash})\left(\frac{\rho_b - \rho_{ash}}{\rho_{0b} - \rho_{ash}}\right). \tag{44}$$

The subscript 0 refers to the initial values of the packed bed.

3.5. Ash formation

Once the char is completely burned, the ash remains. Mathematically ash density is set to the current value of solid density once the char density decreases to less than 5% of its maximum value. The ash is considered to be inert with no participation in the energy equation, has negligible resistance to flow and high porosity.

3.6. Numerical method

The transport equations were numerically solved using the commercially available computational fluid dynamic code, FLUENT 6.0.2. FLUENT uses a control-volume-based technique. The pressure and velocity coupling are done through the continuity equation by use of the SIMPLEC [51] algorithm. The second order scheme, QUICK [52], was chosen for momentum flux calculation through an implicit segregated solver. In order to handle the multi-phase media; FLUENT was customized by utilizing its User Defined Function [53]. This was necessary to separately calculate the changes in both the gas and solid phase temperatures.

4. Results and discussion

Since the gas diffusion has an important role in the rate of oxygen to reach the surface of tobacco shreds and consequently the rate of char oxidation, we first apply the same mathematical model to determine the gas diffusion coefficient through a given wrapper paper. And then we derive a correlation between wrapper paper permeability, which is usually known, and its gas diffusion coefficient. As a less complex case, we apply our model to predict the transport of gases through an unlit cigarette using the derived gas diffusion coefficient. And finally we model a filtered cigarette during the process of static and forward smoldering.

4.1. Paper gas diffusivity

Paper diffusivity plays and important and critical role in determining the yields and composition of products leaving the cigarette filter; thus, it has to be treated very thoroughly. Diffusion coefficient of gases through a cigarette wrapper paper is measured by Drake et al. [54]. They measured the diffusion coefficient of carbon monoxide in a carbon monoxide/nitrogen mixture through the paper using a specially constructed diffusion

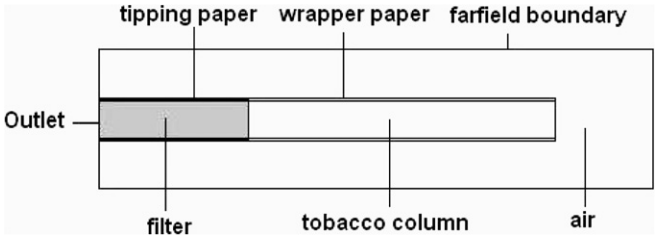

Fig. 2. Schematic of the computational domain for cigarette.

Table 3
Results of grid study comparison

	Base case	Case-1	Case-2
Grid size			
Domain radius (mm)	15	30	15
Domain length (mm)	120	140	120
Mesh size (mm) in cellulose column	0.5	0.5	0.3
Parameter		Maximum difference with respect to the base case (%)	
Max solid temperature (°C)	1212	3.4	7.1
Max gas temperature (°C)	1185	3.1	6
Max velocity in the coal (m/s)	0.58	1.7	6.7
Mass fraction of CO at outlet	5.1e−7	3.9	17.6
Mass fraction of CO_2 at outlet	2.52e−6	19.9	15.7
Mass fraction of H_2O at outlet	1.03e−6	10.7	16.5
Mass fraction of O_2 at outlet	7.45e−6	0.5	7.2
Rate of pyrolysis over cellulose column	4.67e−6	0.6	7.1
Rate of char oxidation over cellulose column	9.85e−7	1.3	12.9
Rate of combustion heat over cellulose column	24.62	1.4	12.9

cell. Briefly, the cell consisted of two identical parallel compartments each of depth $D_c = 3.22$ mm, separated by the paper under test, $L_c = 0.038$ mm thick, $B_c = 3.22$ mm wide, and $X_c = 20$–140 mm length. A gaseous mixture of CO_{inlet} % v/v of carbon monoxide in nitrogen with a flow rate of V_{inlet} cc/s was passed into one compartment of the cell, while nitrogen was flowed at the same rate into the other compartment. As the gas streams flowed through the cell, diffusion through the paper occurred. The concentration difference in mixing-cup concentration ($\Delta CO_m/CO_{inlet}$ % v/v) between the two gases was measured, under a variety of conditions of different gas flow rates, compartment depths, and lengths of paper exposed to the gas streams, as they emerged from the cell. Here, we reproduce their experiments numerically and then, applying linear interpolation and least square techniques on the results, we match the numerical results with experimental ones to find the gas diffusion coefficient through the paper. Since $B_c \gg L_c$ and $B_c \gg X_c$, a two-dimensional model is adapted. Fig. 1a shows the schematic of the computational domain.

The numerical experiment was performed for different flow rates and paper length, for a total of 64 combinations and $\Delta CO_m/CO_{inlet}$ was calculated. Minimizing S, the difference between numerical and experimental results, for all 64 cases leads to the gas diffusion coefficient through the paper:

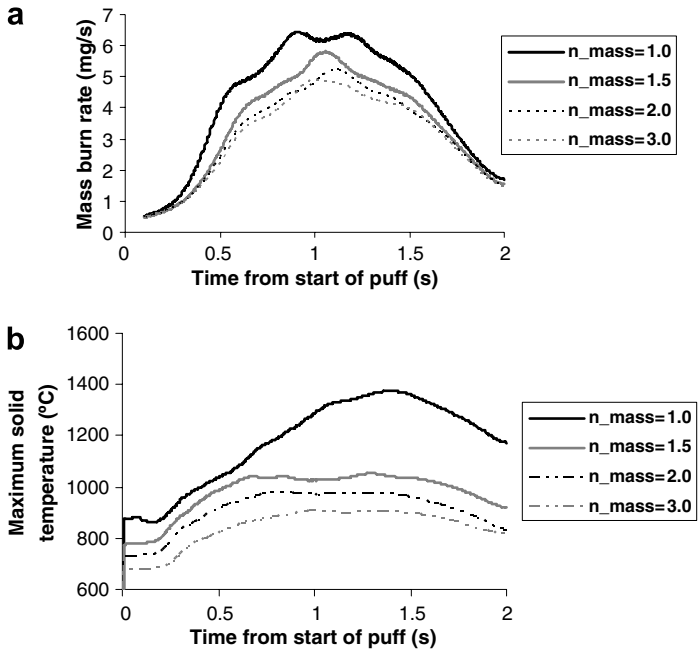

Fig. 3. Simulation results for the puffing period: (a) mass burn rate, (b) maximum solid temperature.

Table 4
Comparison of experimental and simulation results

	n_mass = 1	n_mass = 1.5	n_mass = 2	n_mass = 3
Sensitivity of solid temperature to mass burn rate				
MBR (mg/s)	8	6.7	6.1	5.9
Max solid temperature (°C)	1380	1048	977	904
	Smoldering		Puffing	
	Experimental	Numerical	Experimental	Numerical
Comparison of experimental and numerical data on smoldering and puffing				
Mass burn rate (mg/s)	~0.92	0.96	~5.9	6.1
Max solid temperature (°C)	775	720	950	960
Max gas temperature (°C)	775	600	850	780

$$S = \sum_{i=1}^{N} [(\Delta CO_m/CO_{inlet})_i^{exp} - (\Delta CO_m/CO_{inlet})_i^{calc}]^2. \quad (45)$$

The above procedure leads to $D_{paper} = 4.68 \times 10^{-7}$ m^2/s, which is very close to the value derived by Drake et al. [54], i.e., 4.5×10^{-7} m^2/s. Even though we both have used the same experimental data, the results are different by 4% because different numerical methods have been applied.

The gas diffusion coefficient is proportional to the square root of paper permeability [55]. Having the paper permeability, $K_{paper} = 7.97 \times 10^{-15}$ m^2, leads to the proportionality factor:

$$D_{paper} = 5.24\sqrt{K_{paper}}. \quad (46)$$

Now applying this coefficient and repeating the same numerical experiment, $\Delta CO_m/CO_{inlet}$ is calculated. The results are depicted in Fig. 1b and shows that numerical results are in a perfect match with the experimental ones.

4.2. Gas transport in an unlit cigarette

Having determined D_{paper}, we calculated the rate of dilution of CO in an unlit cigarette and compared the results with the experiments done by Baker and Crellin [56].

They used unfiltered, 69 mm long and 8 mm in diameter cigarettes for their study. The cigarette wrapper paper was about 0.038 mm in thickness with a permeability of 8×10^{-15} m^2. In experiments a mixture of 9.6% v/v carbon monoxide in nitrogen was drawn through the cigarettes by a small vacuum pump. Different lengths of the central portion of the cigarette were exposed to air by wrapping impervious vinyl tape round the remainder of the tobacco rod.

Fig. 1c shows the computational domain simulating the experimental setup. The pressure at cigarette tip is not atmospheric; therefore a fictitious inlet section is added to compensate for the pressure drop up to the cigarette tip. This pressure drop is induced by the rotameter and the tubing installed upstream. Since pressure drop across the rotameter and tubing is proportional to flow velocity (laminar flow), a porous media with a given permeability can be a close substitute. The pressure at cigarette inlet is not known from the experimental data [56]. The flow rate through the wrapper paper not only depends on the physical properties of the cigarette and cigarette outlet flow rate, but also depends on the inlet pressure. For a given setup and dilution ratio, the inlet section permeability, K_{inlet}, was set to gain the same convective dilution ratio numerically. Here, tobacco column and wrapper paper are treated as porous media and Eqs. (1) and (2) are applied for momentum and species transport.

At inlet and far field the ambient pressure at the outlet the velocity is set. The experimental data correspond to cases where the cigarette was subject to an ambient cross flow. Here, we adapt a 3D computational domain. In this case the vertical component of velocity on the lower portion of the cylindrical far field surface was set to the given value while symmetric boundary condition was set on the side walls of the far field.

Applying the gas diffusion coefficient calculated in the previous section and setting $K_{inlet} = 9.35 \times 10^{-11}$ m^2, the total rate of carbon monoxide dilution was predicted for different cross flow velocities. The dilution is due to both convection and diffusion mechanisms. The contribution of convection is equal to the mass flow rate through the wrapper paper divided by mass flow rate at the outlet. Consequently, the dilution due to diffusion is calculated and is depicted in Fig. 1d. It is noticed that the numerical results are in a good agreement with the experimental ones.

4.3. Static and forward smoldering

4.3.1. Grid study

Due to the presence and effectiveness of buoyancy forces, the flow dynamics of smoldering and puffing a cigarette becomes a three-dimensional problem except for special case when the cigarette axis is aligned with gravity. However, the problem is symmetric with respect to a vertical plane passing through the cigarette axis. Thus, the computational domain comprises half of the physical domain. Fig. 2 shows the computational domain along the plane of symmetry.

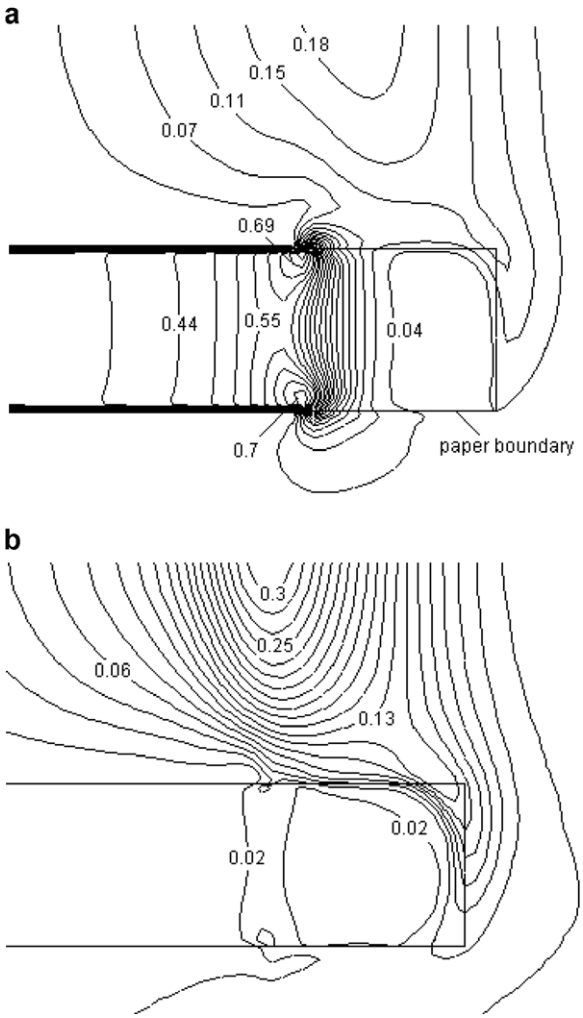

Fig. 4. Velocity (m/s) contours (a) during puffing and (b) during smoldering on plane of symmetry (m/s).

In order to make sure that the extent of computational domain and the mesh size do not change the results considerably, a grid study was performed on cigarette type beds with cellulose shreds to find the proper domain and grid size. The process of cigarette puffing is a transient problem and to simulate the behavior of cigarette during puffing, the program has to be run for tens of seconds. On the other hand, the problem is highly non-linear and stiff, and thus the time step has to be limited to at most 0.005 s to attain convergence. Therefore, in order to be able to simulate cigarette puffing in a reasonable time, we have to reduce the domain and coarsen the grid as much as possible.

The grid study was performed on three grids. The base grid was chosen to have a cell size of 0.5 mm in cellulose column and its far field boundary was set at a distance of 11 mm from the cigarette periphery and 20 mm from the cigarette tip. The specification of the other grids is shown in Table 3.

The numerical simulation starts with lighting the cigarette and simultaneously increasing the outlet flow, then keeping the flow at a constant value of 17.5 cc/s. After 14 s of continuous puffing we compare the results. The spatial comparison of solid temperature, gas velocity, gas temperature, the smoke constituents at cigarette outlet, the rate of pyrolysis, char oxidation, and heat produced due to combustion over the cellulose column are depicted in Table 3. Even though the difference for smoke constituents is as high as 20%, still it is in the range of the deviation of experimental results [57]. Therefore, the base grid is coarse enough for the numerical simulation. However, the computational effort for numerical simulation of the process of cigarette puffing is

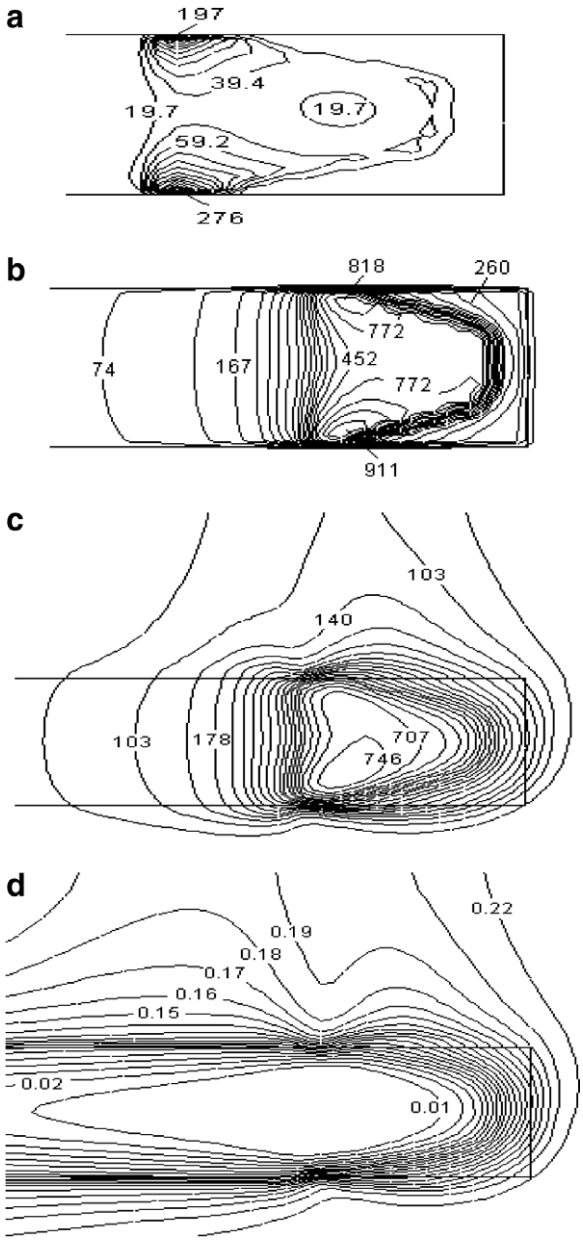

Fig. 5. Contours of (a) heat of combustion (W), (b) solid temperature (°C), (c) gas temperature (°C), and (d) oxygen mass fraction on the plane of symmetry during puffing.

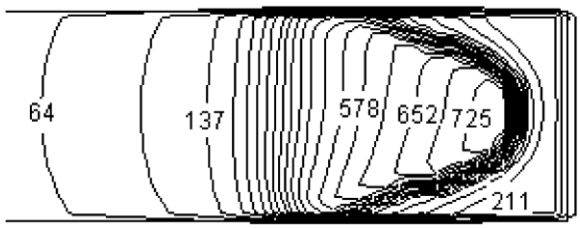

Fig. 6. Contours of solid temperature during smoldering on plane of symmetry (°C).

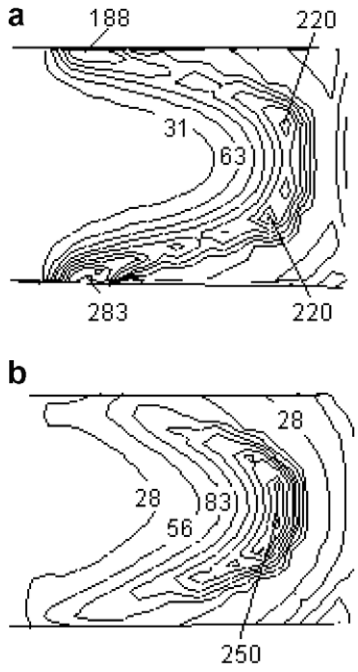

Fig. 7. Contours of $|T_s - T_g|$ (°C) during puffing (a) and smoldering (b).

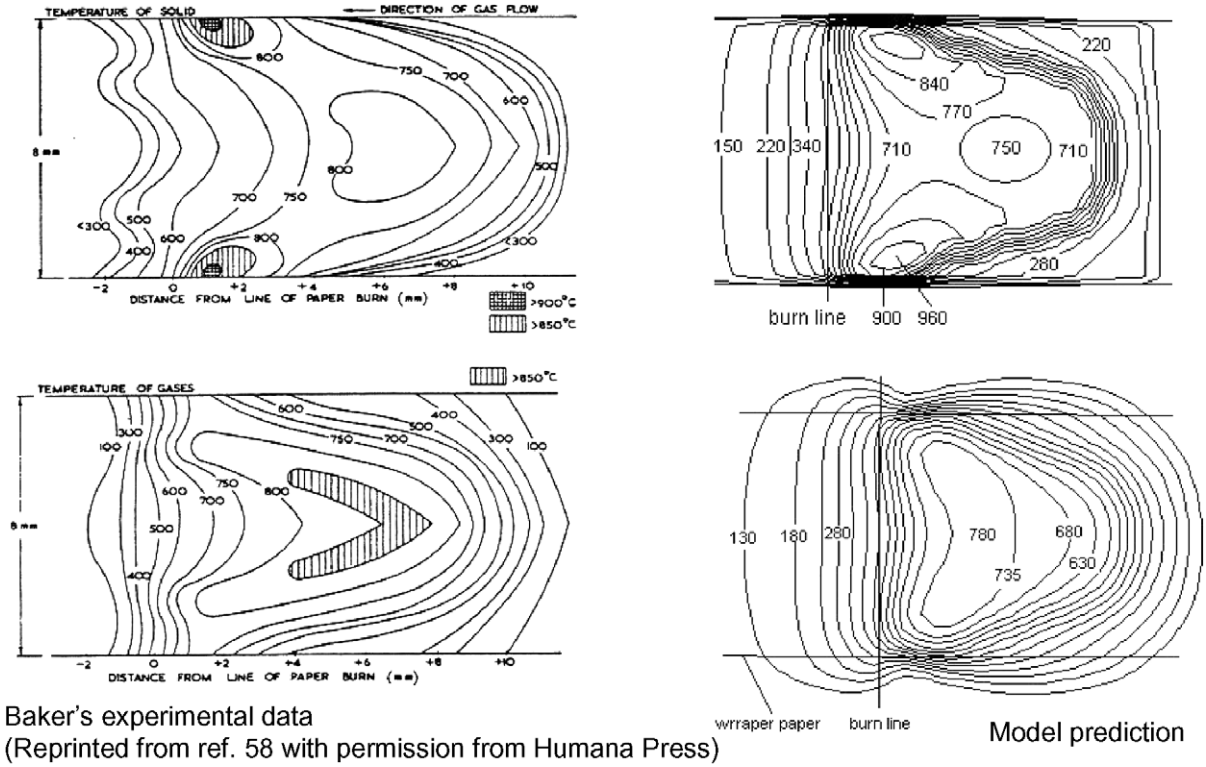

Fig. 8. Comparison of the experimental and simulation results for the solid and gas temperatures on a horizontal plane passing through the cigarette axis (°C); experimental results reprinted from Ref. [58] with permission from Humana Press.

exceedingly high even with the base grid and it takes several days to finish a single puff simulation on a two processor machine.

4.3.2. Mass transfer correction factor

The mass transfer correction factor is determined by matching the numerical and experimental results. We consider four cases namely $n_{mass} = 1$, 1.5, 2, and 3. The case $n_{mass} = 1$ refers to no pore diffusion resistance. In all four cases the data relating to the second puff of a conventional cigarette was recorded and compared with experiment. Each puff cycle is composed of a 2 s sinusoidal puff with a total puff volume of 35 cc and followed by 58 s smoldering interval. The cigarette was held horizontally and lit for the first puff and then the computation was continued to cover the second puff. Fig. 3a and b shows the maximum solid temperature and total mass burn rate of tobacco shreds during the second puff, respectively. It is noticed that for $n_{mass} = 1$ and 1.5 the burn rate is relatively high. The difference in the shape of the curves is related to multi-precursor pyrolysis model of the tobacco that will be explained later. The average mass burn rate during the puff period is calculated and compared with the experimental data in Table 4. It is noticed that $n_{mass} = 1$ overestimates the burn rate while $n_{mass} = 2$ reproduces more realistic results. The measured maximum solid temperature during the puff is reported to be close to 950 °C. Fig. 3b shows that the cases $n_{mass} = 1$ and 3 lead to unrealistic high and low solid temperatures while $n_{mass} = 2$ results are closer to the experiments. The case $n_{mass} = 2$ has reproduced a good match with the experimental data and, therefore, is used in the numerical simulations.

4.3.3. Smoldering and puffing of a cigarette

In this section the results, of the second puff followed by smoldering, is presented. The puff profile is sinusoidal with duration of 2 s and a puff volume of 35 cc. In order to show the behavior of cigarette during puffing and smoldering, the data corresponding to the peak of the puff (one second after the start of the puff) and three seconds after the end of the puff (smoldering) are chosen.

Once the cigarette is lit, heat delivered by the lighter and the heat generated during char oxidation, is propagated downstream mainly by the hot gas carrier. As the cigarette heats up and its temperature rises, the wrapper paper temperature also rises. In our model we have considered the wrapper paper as a porous media but its combustion is not modeled yet. Rather it is assumed that once the paper temperature exceeds 450 °C it burns and converts into ash.

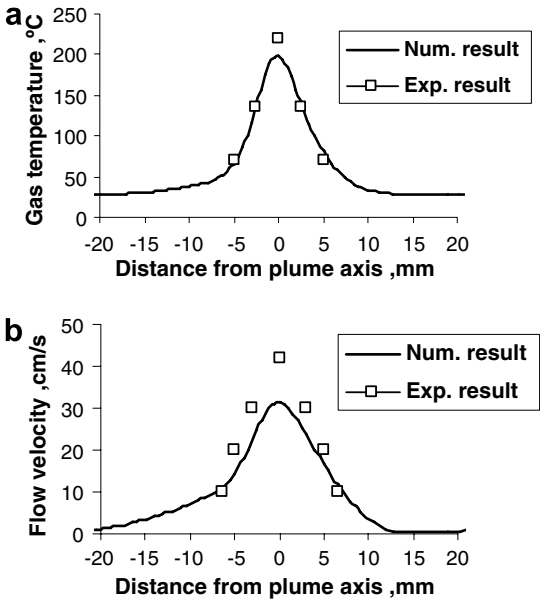

Fig. 9. Gas temperature (a) and velocity (b) in smoke plume during smoldering.

The process of cigarette and wrapper paper burning and the change of its temperature have a pronounced effect on flow pattern in the burning zone and its close neighborhood. As paper is burned and is converted into ash, its permeability drastically increases and its resistance to flow becomes negligible. On the other hand, in the cigarette coal there are two parameters that contribute to it's resistance to air flow. The bed density is lower in the burned cigarette than unburned cigarette; therefore its permeability is higher leading to lower pressure drop. The rise in the gas temperature increases the viscosity of gases that leads to higher pressure drop. These two counter acting effects along with production of high velocity gases during pyrolysis and char oxidation causes the cigarette coal to attain a comparatively higher resistance to flow. Thus, unlike the case of an unlit cigarette where the flow uniformly passes through the cigarette tip in all directions, the flow is mainly by-passed by the coal and enters the tobacco column primarily through the coal periphery and at the location where the paper is just burned. The line passing through this cross section is called paper burn line. Paper burn line indicates the location of minimum resistance to flow and maximum incoming flow velocity. This behavior is clearly demonstrated in the velocity contours shown in Fig. 4a corresponding to peak of the puff. Velocities as high as 0.7 m/s, slightly above the burn line are noticeable. Fig. 4b shows the velocity contours for smoldering. Due to high pressure drop inside the coal, the flow velocity inside the coal is small. This results in a similar flow distribution, for both smoldering and puffing, in inner parts of the coal and the main difference appears on the burn line. The gases in the smoke plume during smoldering have comparatively higher velocity in the absence of a flow drawn into the cigarette column.

In a cigarette, the rate of char oxidation is controlled by the rate of oxygen mass transfer to the char surface [31]. Therefore, the rate of char oxidation is expected to be at maximum at burn line where the incoming flow is bringing in fresh oxygen into that region. Fig. 5a shows the distribution of the rate of char oxidation at the peak of a puff (1 s after puffing starts). The energy released due to char oxidation is delivered to the solid, there by increasing its temperature. Note the contours of char oxidation are similar to the solid temperature contours (Fig. 5b) and also their maximum values fall in a similar region. The highest solid phase temperature occurs at the coal periphery just in front of the paper burn line, where the air influx into the coal is at maximum. The gas temperature in the same region is relatively cooler, as can be seen in Fig. 5c, and it is higher in the inner zone where the flow velocity is lower. As discussed in previous section, the process of char oxidation is mass transfer controlled. We know the cigarette coal is composed of a porous char which provides a large solid–gas interfacial surface area. This makes the mass transfer rate to be high enough to establish an oxygen deficient zone through out the coal except at burn line and on coal surfaces, This trend is shown in Fig. 5d, where the oxygen contours are depicted during puffing. The availability of oxygen on paper burn line during puffing is due to inflow of fresh air. Contours of solid temperature during smoldering in the coal region are shown in Fig. 6. Higher temperatures are observed on the surface of the coal region during puffing and smoldering. This is primarily due to availability of oxygen on the coal surface, during both puffing and smoldering, primarily due to the flow driven by natural convection. During puffing the rate of heat production is almost six times higher than during smoldering. This causes the solid and gas temperatures to be higher during puffing. It is believed that high heating rates and high local gas velocities does not allow the solid and gas temperatures to reach a thermal equilibrium. In order to find the extent of non-equilibrium, the absolute difference between solid and gas temperatures at peak of puff and during smoldering were calculated and are shown in Fig. 7a and b. It can be noticed that the maximum smoldering, indicating thermally non-equilibrium during these two phases. The temperature difference is low only in the central part of the coal, where the gas velocity is very low for smoldering and puffing (see Fig. 4a and b). Therefore, treating solid and gas energy equations separately, is the proper choice for this problem.

In order to validate the mathematical model, the process of smoldering and puffing of a conventional filtered cigarette was numerically simulated. The maximum solid and gas temperature and also the average mass burn rates during smoldering and puffing are depicted in Table 4. Although the differences would be as high as 20%, the comparison shows that the numerical results are in very good agreement with the experimental results of a typical cigarette.

Baker [58] has measured the gas and solid temperatures in a burning cigarette and produced corresponding contours for a cigarette. Since the data correspond to a horizontal plane passing through the cigarette axis, here we have also produced numerical data on the same plane. The results corresponding to the peak of the puff are shown in Fig. 8. Given the fact that the tobacco blend of the numerical model and the experimental

one is not the same, it can be noticed that the model has reproduced the basic features of the temperature distribution and is also in good agreement with the experimental results quantitatively.

The buoyancy causes an upward flow around the cigarette coal. Therefore, the availability of oxygen is higher on the lower surface of coal than its upper surface, implying higher rate of char oxidation on the lower surface (Fig. 5a). This higher level of oxygen results to a relatively higher gas velocity, solid temperature and gas temperature on the lower side, as is clearly noticed from Figs. 4a and 5b and c, respectively. During puffing most of the gases produced due to pyrolysis and char oxidation are directed toward the outlet and the rest go into the smoke plume.

The temperature and velocity of smoke plume one centimeter above the coal of a smoldering cigarette was calculated and is compared with the experimentally measured data in Fig. 9a and b. The gas temperatures calculated numerically are in good agreement with the values obtained experimentally. On the other hand, the numerical results of velocity are comparatively lower than the experimental one. This is due to the lower temperatures predicted by the model, lower than the measured data, during smoldering. Analysis of the data shows that the coal is overcooled by the effect of radiation and replacing the simple coal-cooling model by a more rigorous model should improve the results.

The rate at which heat front (combustion) propagates can be calculated from the average mass burn rate. The average mass burn rates during smoldering and puffing are calculated to be 0.92 and 6.1 mg/s, respectively. Based on the geometry and packing density of the cigarette given in Table 1, the equivalent linear burn rates are 0.083 and 0.5 mm/s. The heat exchange between solid and gas is the main mechanism of movement of heat front during smoldering. Fig. 10a and b shows the contours of heat exchange between solid and gas at the peak of the puff. The positive sign refers to gas gaining energy from solid. It is demonstrated that just above the burn line where the rate of char oxidation is highest and on the periphery region close to burn line where the heat transfer coefficient is larger, is where the gas experiences maximum heat gain. As the hot gases move downstream into the tobacco column, they immediately deliver most of their heat to lower temperature solids within a few millimeters, due to higher heat capacity of the tobacco shreds, and reach equilibrium with ambient temperature. This causes the pyrolysis of tobacco shreds just below the burn line. On the other hand the gases produced in the coal upper region, which are not affected by the suction, induced at the outlet, flow toward the outer region of the coal and deliver their heat to the solid as they leave the coal (Fig. 10b).

The heat propagation through the tobacco column can also be shown by tracing the temperature change of a fixed tobacco particle. We consider two tobacco particles positioned on the cigarette axis and periphery on a line passing through the paper burn line as we start the puff. Fig. 11 shows that both particles experience a sharp change in their temperature rising to 740 and 920 °C with heating rates as high as 300 and 500 K/s. As the heat wave passes through the tobacco column, the particles gain heat and their temperature increase. The maximum temperature of particles does not necessarily coincide with maximum velocity of puff profile which happens at time = 1 s. This delay is even larger for the particle on the center. At the center the temperature and heating rates are lower and it takes a longer time to produce char and burn it, resulting in a bigger lag. After the end of the puff the temperature of the particle at periphery falls down faster, mainly due to radiation cooling and char depletion.

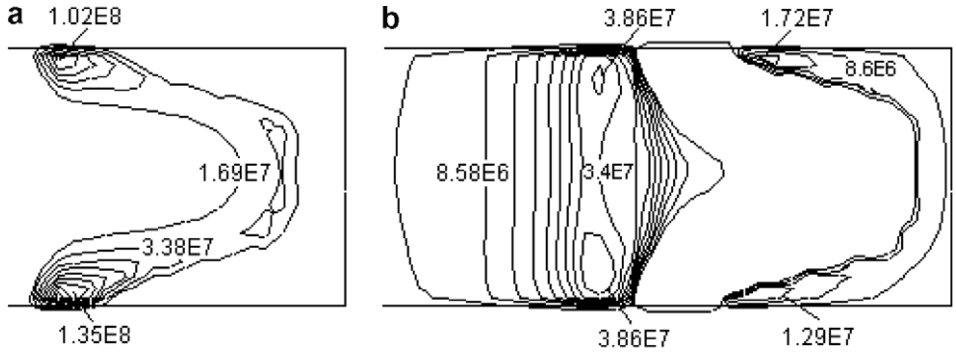

Fig. 10. The rate of heat (W) lost (a) and gained (b) by solid particles during puffing.

Fig. 12 shows the distribution of the density of raw tobacco, available volatile material and char of tobacco shreds along the cigarette axis at the peak of the puff. The initial decrease in the density of raw tobacco at about 6 mm behind the burn line is due to evaporation of its moisture. As we get closer to the burn line and temperature rises to 450 °C, the tobacco starts to pyrolize and there is a further decrease in its density. This region extends to about 3 mm behind the burn line and beyond which burning of tobacco takes place. At the same time char is produced during pyrolysis and is consumed due to oxidation. The overall effect is a sharp increase in char density within 3 mm, almost plateaus out in the interior region of the coal due to lack of oxygen and burns faster towards the coal surface where fresh oxygen is available. This causes an almost plateau in the solid density profile as is clearly noticed in Fig. 12.

The constituents of mainstream smoke are analyzed to determine the amount of various gas and vapor that come out of the filter. We obtained the total amount of each of the main constituents of cigarette smoke coming out of the outlet, during the puff, by integrating the instantaneous mass flow rate over the 2-s puff cycle, and have presented that against the experimental results in Table 5. The experimental and numerical results are in a reasonable agreement for most of the components. The main difference between numerical and experimental results is observed for carbon dioxide. The mainstream smoke CO_2/CO is typically about 3 whereas the ratio predicted by our model is 2.1. The present model does not consider the homogeneous gaseous reactions during char oxidation including carbon monoxide oxidation and water–gas shift reactions. Also the catalytic effect of alkaline metals and gasification of carbon by water vapor and CO_2 has also been ignored. These factors have considerable effect on the concentration of CO and CO_2 in mainstream smoke. The primary reasons for ignoring gas phase reactions were the lack of fundamental understanding under the cigarette smoking and complication in reaching a stable and more accurate result in simulation. We should add to this the fact that the pyrolysis experiments are normally performed under conditions of heating rates and residence times which are different from the conditions inside a burning cigarette. For example Fig. 11 shows that during puffing the heating rates are as high as 500 K/s while the pyrolysis kinetic parameters used in our model are derived from experimental data with about 1 K/s heating rate [27,28]. It has been well known and demonstrated that the estimation of kinetic parameters at low heating rate must be corrected before they are used for high heating rates [28]; otherwise, an over or under-estimation in the rates are expected at high heating rates. We believe all these factors and an uncertainty in thermo-physical properties of the substrates are the primary cause for the difference in numerical and experimental values. Since the formation, adsorption and transport of aerosol particles through the cigarette column and consequently water vapor condensation into aerosol particles are not modeled, the deviation between the two results for particulate phase and water vapor is larger.

Fig. 13a shows the CO mass fraction contours on the plane of symmetry at peak of the puff. The gaseous species produced during puffing mainly leave the cigarette outlet as mainstream and the rest go into surrounding air as side stream. As the gaseous species move along the tobacco column, they are continuously diluted by a combination of the gas diffusing out and air diffusing in through the wrapper paper. The diffusion of CO through the wrapper paper can be clearly noticed from the figure.

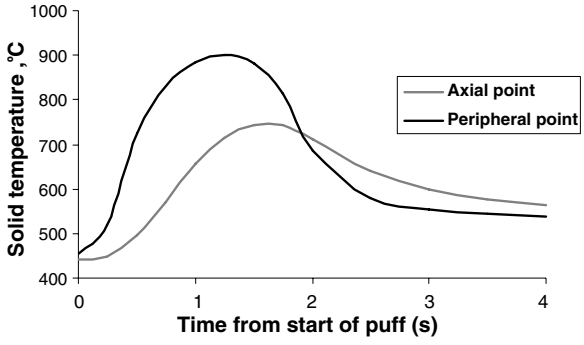

Fig. 11. The time variation of tobacco particles during puffing and smoldering.

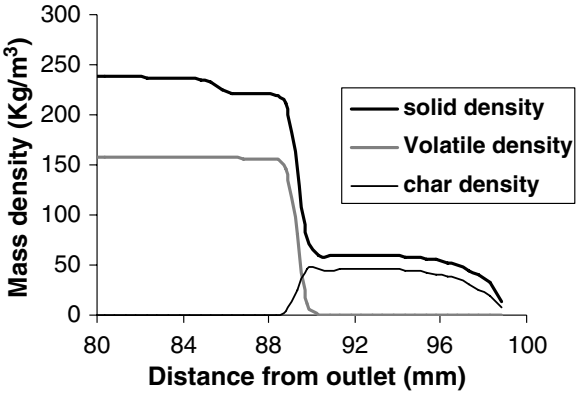

Fig. 12. The distribution of solid, volatile and char density along the cigarette axis at the peak of the puff (1 s after starting of a puff).

Table 5
Some experimental and numerical data on mainstream smoke constituents

	Smoke constituents' yields in mainstream smoke					
	Oxygen	Carbon dioxide	Carbon monoxide	Vapor phase	Particulate phase	Nitrogen
(A) Comparison with a given brand (% by weight/cigarette smoked)						
Exp	13	12.5	4	4	4.5	62
Num	12	13	4	5	8	58

	Oxygen	Carbon dioxide	Carbon monoxide	Nitrogen	Water vapor	Acetaldehyde	Nicotine
(B) Comparison with a range of cigarettes (mg/cigarette smoked)							
$(Exp)_{Max}$	70	50	23	320	14	1.2	2.3
Num	68.9	36.4	15.7	293	17.8	1.1	1.4
$(Exp)_{Min}$	50	20	10	280	3	0.5	0.8

Fig. 13b and c shows the mass fraction of CO on the upper surface and on the axis of the cigarette respectively at different times. The time = 0 corresponds to the smoldering and start of puffing. During smoldering the CO mass fraction along the axis is maximum at $x = 0$ (burn line), and within 10 mm it decreases sharply to zero due to dilution. The portion of the curve in the coal zone slowly decreases because CO dilution is partially compensated by CO production during char oxidation and finally goes to zero outside the coal. The CO profile on the surface is a typical plume profile and its maximum is located in front of the burn line. At the peak of the puff the heat front has moved and this causes the CO on the axis to increase sharply and its maximum moves to the new location as burn line moves. The CO produced is convected by the flow, and, simultaneously and slowly is diluted by inflow of air through the wrapper paper and diffusion of CO out as it moves along the tobacco column. This trend causes, unlike velocity profile which is flat in the tobacco column, the CO profile to be parabolic as shown in Fig. 13a. In Fig. 13b and at time = 1 s, the CO concentration on the surface is lower at burn line due to inflow of air and a sharp increase of CO afterward. It is noticed that during puffing and even after the puff is finished, the CO concentration is not zero.

The mass flow rate of CO during the 2-s puff is shown in Fig. 14a. In one case the cigarette is filled with tobacco and in another with cellulose. The CO and CO_2 mass flow rates for the case of cigarette are higher. It can be noticed that there is a delay between start of the puff and delivery of CO or CO_2 at the outlet. As was mentioned before, during smoldering the CO concentration goes to zero within one centimeter from the coal base. Therefore, it takes time for the gases that produced in the coal to be transported to the cigarette outlet. This time is a function of puff velocity profile and the distance between burn line and outlet. In the present case, the estimated delay time based on puff velocity and distance between the burn line and outlet is 0.4 s, which is nearly the same as in Fig. 14a. Even though we have applied a sinusoidal puff profile, the CO and CO_2 and other mainstream smoke constituents do not essentially follow a sinusoidal curve. This is due to

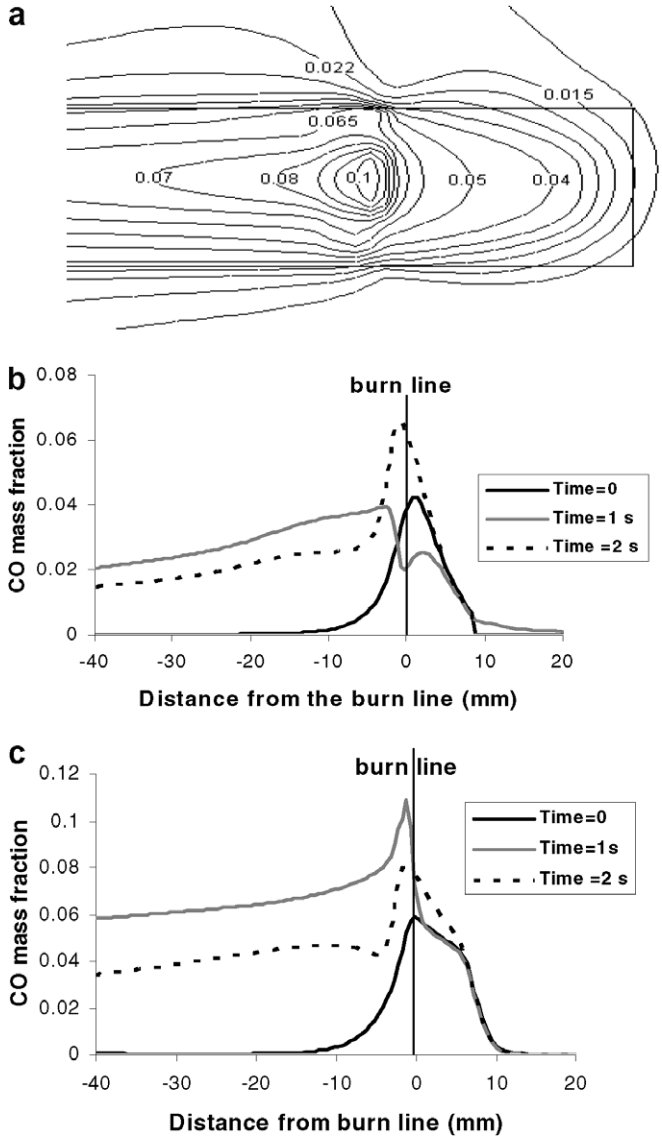

Fig. 13. (a) Contours of CO mass fraction during puffing; (b) distribution of CO mass fraction on cigarette surface at start, peak, and end of puff, and (c) distribution of CO mass fraction on cigarette axis at start, peak, and end of puff.

the fact that the flow pattern of these constituents is not only dependent on the flow velocity but also on the generation of these components. Also it is noticed that CO shows more variation during the puff. The main reason is the way that tobacco or cellulose is pyrolized. To show this we consider the mass burn rate (MBR). The loss in the weight of column comes as a result of three processes namely moisture evaporation, substrate pyrolysis and its char oxidation. Thus, the mass burn rate (MBR) is composed of three rates, namely moisture evaporation, substrate pyrolysis and its char oxidation. The rate of pyrolysis is predominant over the moisture evaporation and, therefore the mass burn rate follows the trend of rate of pyrolysis as is clearly noticed in Fig. 14a. On the other hand the trend of pyrolysis and decomposition into volatiles such as CO and CO_2 is dependent on the model adapted for pyrolysis. In the present model, pyrolysis is defined in terms of precursors that behave differently at different temperature and heating rates. Some of these precursors deplete faster at lower temperatures and others evolve at higher temperatures and under restricted conditions. For the case of CO, this is shown in Fig. 14b. To better illustrate this, we have taken two tobacco particles, one on the axis

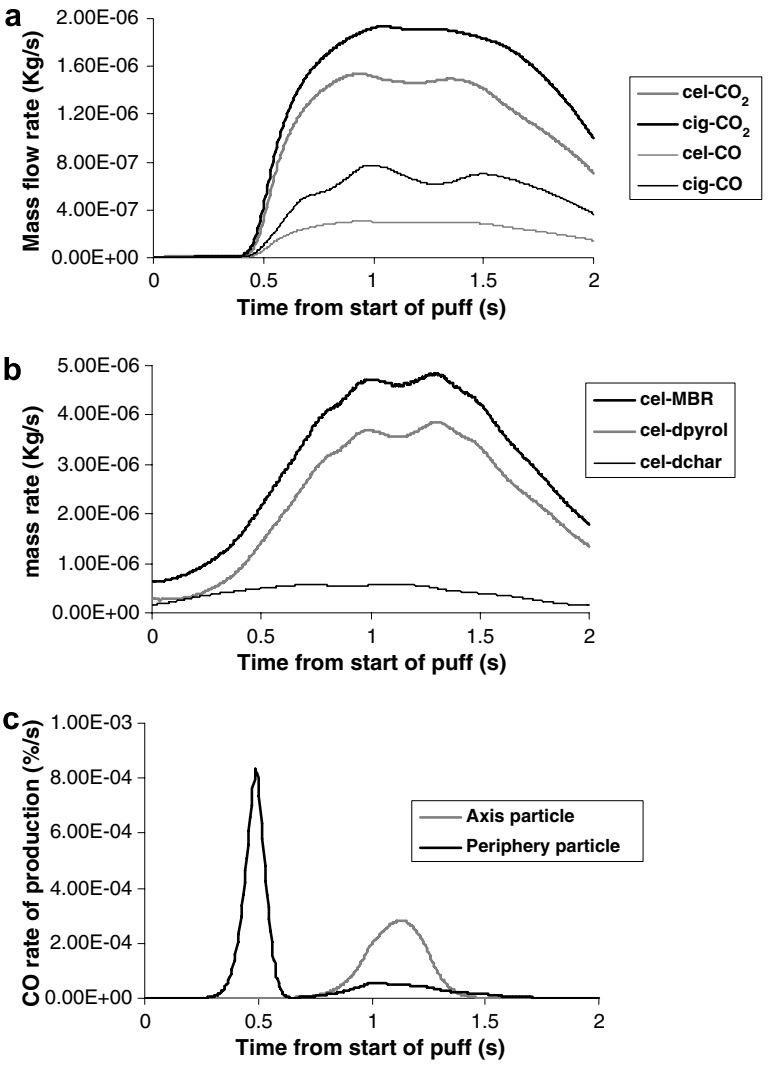

Fig. 14. (a) Mass flow rate of CO at outlet during puffing, (b) rate of mass burn, pyrolysis, and char oxidation during puffing, and (c) rate of CO production during tobacco pyrolysis.

and the other on the surface of cigarette. We have imposed the temperature history profiles on the axis and the surface of cigarette as shown in Fig. 11 on these two tobacco particles. This shows that the particles sitting on the burn line depletes fast, almost within the first half second of the puff, while the one sitting on the axis start pyrolysis at about 0.7 s into the start of the puff. Thus, the sources of CO production over the pyrolysis zone contribute differently during the puff. This is the main cause of experiencing ups and downs in CO (Fig. 14b) and other species in the main stream smoke, and, in general the total rate of pyrolysis (Fig. 14b). CO is represented by three precursors in the tobacco pyrolysis and only one precursor in cellulose pyrolysis and therefore it explains the different rates of CO for cellulose and tobacco at outlet. The precursor assumption for CO production comes as a result of the starting material chemical composition. For cellulose which is a pure compound, a single precursor for CO production during pyrolysis is a good assumption as the derivative of the production curve (rate) gives a single peak. For the tobacco which is composed of various chemicals such as sugar, pectin, cellulose, lignin and soluble and insoluble oxalate, carbonates, etc., a multiple source (precursors) is necessary to fit the experimental data to kinetic models.

A numerical simulation was conducted on two different types of cigarettes, one filled with tobacco shreds and the other with cellulose shreds. All other conditions were kept the same. Both simulations were "smoked"

Table 6
Comparison of the numerical results obtained for different biomass materials

Parameter	Cellulose	Tobacco
Max solid temperature (°C)	1098	980
Max gas temperature (°C)	1047	817
Max velocity in the coal (m/s)	0.89	0.7
Mass fraction of CO at outlet	3.8e−7	8.78e−7
Mass fraction of CO_2 at outlet	1.90e−6	2.47e−6
Mass fraction of H_2O at outlet	5.96e−7	7.25e−7
Mass fraction of O_2 at outlet	5.72e−6	4.65e−6
Rate of pyrolysis over biomass column (kg/s)	1.35e−6	1.31e−6
Rate of char oxidation over biomass column (kg/s)	8.4e−7	7.2e−7
Rate of combustion heat over biomass column (W)	20.8	12.6
MBR (kg/s)	6.2e−6	6.1e−6

under the same puff profiles and the results for both the fillers used during the second puff are compared in Table 6. The char form cellulose has higher heating value and produces more heat per unit mass of char burned, comparing to tobacco char. This causes the rate of heat generation to be 54% higher and thus the gas and solid temperatures for the cellulose to be higher. The yield of CO and CO_2 due to cigarette thermal decomposition [27] is 10 and 12 times larger than the cellulose [26], respectively. On the other hand, Table 6 shows that their rate of char oxidation is closer and consequently their rate of CO and CO_2 production due to char oxidation are closer. Adding these together leads to higher CO and CO_2 production in case of cigarette burning. The burn rate is about the same for the two cases. Unit mass of cellulose has comparatively more ash and less char and volatile material and this has adverse effect of higher rate of pyrolysis due to higher solid temperature. Fig. 15a and b shows the char density at the peak of puff. It can be noticed the shape and magnitude of the two figures are different; the tobacco coal is more of a conical shape compared to cellulose coal which is flatter. Since cellulose has a higher char mass per unit mass of raw material, we expect it to have higher char densities. The cellulose has more ash; and even though its char burn rate is slightly higher during puffing, most of the char is oxidized during smoldering itself. Thus, we have relatively higher solid density spread on the outer zone of the coal. This makes the oxygen deficient zone to be larger for the case of cellulose and therefore the coal is burned more uniform across the cigarette.

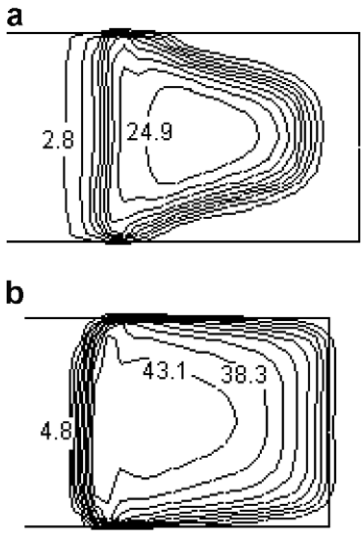

Fig. 15. The car density of tobacco (a) and cellulose (b) coals during puffing (kg/m^3).

5. Conclusion

For the first time a 3D model based on the principles of conservation of mass, momentum and energy for geometry similar to a cigarette was developed that successfully simulates the puff-smoldering cycles of a lit-end cigarette. The mass, momentum, energy, and species transport equations are solved in a discretized computational domain using a commercially available CFD code. The simulation results show that the model reasonably reproduces the major features of a burning cigarette during smoldering and puffing. Results include the velocity profiles, gas and solid temperatures, coal shape, burn rates, profile and transport of gas and vapor species throughout the packed bed, dilution through the wrapper paper and ventilation in the filter section, and the mass fraction of some pyrolysis and oxidation products in the mainstream and sidestream flows. Results show the significance of diffusion mechanism in dilution of gaseous species transported through the cigarette. The solid and gas temperatures as well as some predicted mainstream smoke constituents by the model for a puffing cigarette are in a reasonable agreement with the existing experimental results. Replacing tobacco with cellulose in the geometry causes an increase in solid and gas temperatures as well as the CO and CO_2 delivery in the mainstream smoke.

Acknowledgements

Authors would like to thank Dr. F. Rasouli for his technical assistance and discussions, and Drs. P. Chen and P. Lipowicz for their helpful comments. Saidi Partnership would also like to acknowledge Philip Morris USA, Inc. for the financial support, and Isfahan University of Technology for extending Dr. Saidi's sabbatical.

References

[1] C. Bruch, B. Peters, A flexible and stable numerical method for simulating the thermal decomposition of wood particles, Chemosphere 42 (2003) 481–490.
[2] W.R. Chan, M. Kelborn, B. Kreiger, Modeling and experimental verification of physical and chemical processes during pyrolysis of a large biomass particle, Fuel 64 (1985) 1505–1513.
[3] R.S. Miller, J. Bellan, Analysis of reaction products and conversion time in the pyrolysis of cellulose and wood particles, Combust. Sci. Tech. 19 (1996) 331–373.
[4] R. Bilbao, J.F. Mastral, J. Ceamanos, M.E. Aldea, Modeling of the pyrolysis of wet wood, J. Anal. Appl. Pyrol. 36 (1996) 81–97.
[5] B. Peters, C. Bruch, Drying and pyrolysis of wood particles: experimental and simulation, J. Anal. Appl. Pyrol. 70 (2003) 233–250.
[6] S.V. Leach, G.G. Rein, J.L. Ellzey, O.A. Ezekoye, J.L. Torero, Kinetic and fuel property effects on forward smoldering, Combust. Flame 120 (2000) 346–358.
[7] M. Fatehi, M. Kaviani, Role of gas-phase reaction and gas–solid thermal nonequilibrium in reverse combustion, Int. J. Heat Mass Transfer 40 (1997) 2607–2620.
[8] A. Egerton, K. Gugan, J. Weinberg, The mechanism of smoldering in cigarettes, Combust. Flame 7 (1963) 63–78.
[9] T.J. Ohlemiller, Modeling of smoldering combustion propagation, Prog. Energy Combust. Sci. 11 (1985) 277–310.
[10] M. Summerfield, T.J. Ohlemiller, H.W. Sandusky, A thermophysical mathematical model of steady-draw smoking and predictions of overall cigarette behavior, Combust. Flame 33 (1973) 263–279.
[11] J. Norbury, A.M. Stuart, A model for porous-medium combustion, Q. J. Mech. Appl. Math. 42 (1989) 159–178.
[12] E.J. Kansa, H.E. Perlee, R.F. Chaiken, Mathematical model of wood pyrolysis including internal forced convection, Combust. Flame 29 (1977) 311–324.
[13] M. Muramatsu, S. Umemura, T. Okada, A mathematical model of evaporation–pyrolysis processes inside a naturally smoldering cigarette, Combust. Flame 36 (1979) 245–262.
[14] H.W. Sandusky, A Computer-Simulated Cigarette Model for Use in the Development of Less Hazardous Cigarette, Ph.D. Thesis, Princeton University, Princeton, NJ, 1976.
[15] D.C. Di Blasi, Modeling and simulation of combustion processes of charring and non-charring solid fuels, Prog. Energy Combust. Sci. 19 (1993) 71–104.
[16] S.E. Yi, M.R. Hajaligol, Mathematical model of smoldering combustion in a carbonaceous porous medium, Part 1 – development of pyrolysis and combustion models for a cylindrical geometry, Fire Sci. 19 (2001) 429–448.
[17] A. Rostami, J. Murthy, M.R. Hajaligol, Modeling of a smoldering cigarette, J. Anal. Appl. Pyrol. 66 (2003) 281–301.
[18] A. Rostami, J. Murthy, M.R. Hajaligol, Modeling of the smoldering process in a porous biomass fuel rod, Fuel 83 (2004) 1527–1536.
[19] M.S. Saidi, M.R. Hajaligol, F. Rasouli, An experimental and numerical analysis of puff hydrodynamics, Beitr. Tabakfosch. Int. 21 (2004) 157–166.

[20] M.S. Saidi, M.R. Hajaligol, F. Rasouli, Numerical simulation of a burning cigarette during puffing, J. Anal. Appl. Pyrol. 72 (2004) 141–152.
[21] L. Shijie, A. Afacan, J. Masliyah, Steady incompressible laminar flow in porous media, Chem. Eng. Sci. 49 (1994) 3565–3586.
[22] S. Ergun, Fluid flow transport through packed column, Chem. Eng. Prog. 48 (1952) 89–94.
[23] F.A.L. Dullien, Porous Media: Fluid Transport and Pore Structure, second ed., Academic Press, New York, 1992.
[24] M.S. Saidi, P.J. Lipowicz, J. Aerosol Sci., submitted for publication.
[25] M. Fatehi, M. Kaviany, Role of gas-phase reaction and gas–solid thermal nonequilibrium in reverse combustion, Int. J. Heat Mass Transfer 40 (1997) 2607–2620.
[26] R.R. Baker, The kinetics of tobacco pyrolysis, Thermochem. Acta 17 (1976) 29–63.
[27] Advanced Fuel Research, Inc., Internal report, October 12th, 2000.
[28] M.A. Wojtowicz, R. Bassilakis, W.W. Smith, Y. Chen, R.M. Carangelo, Modeling the evolution of volatile species during tobacco pyrolysis, J. Anal. Appl. Pyrol. 66 (2003) 235–261.
[29] E.M. Suuberg, Approximate solution technique for non-isothermal, Gaussian distributed activation energy models, Combust. Flame 50 (1983) 243–245.
[30] Z. Du, A.F. Sarofim, J.P. Longwell, L. Tognotti, The CO/CO_2 ratio in the products of the carbon–oxygen reaction, in: Fundamental Issues in Control of Carbon Gasification Reactivity, Kluwer Academic Publishers, Netherlands, 1991, pp. 91–106.
[31] M. Muramatsu, S. Umemura, T. Okada, Consumption of oxygen and heat evolved during natural smolder of a cigarette, J. Chem. Soc. Jpn., Chem. Ind. Chem. (1978) 1441–1448.
[32] T. Kashiwagi, H. Nambu, Global kinetic constants for thermal oxidative degradation of a cellulosic paper, Combust. Flame 88 (1992) 345–368.
[33] B. Peters, C. Bruch, Drying and pyrolysis of wood particles: experiments and simulation, J. Anal. Appl. Pyrol. 70 (2003) 233–250.
[34] E. Tsotsas, E. Martin, Thermal conductivity of packed beds, a review, Chem. Eng. Process 22 (1987) 19–37.
[35] G.J.A. Cheng, B. Yu, P. Zulli, Evaluation of effective thermal conductivity from the structure of a packed bed, Chem. Eng. Sci. 54 (1999) 4199–4209.
[36] M. Kaviany, Principles of Heat Transfer in Porous Media, second ed., Springer, New York, 1995.
[37] D.J. Gunn, Axial and radial dispersion in fixed beds, Chem. Eng. Sci. 42 (1987) 363–373.
[38] D. Vortmeyer, Axial heat dispersion in packed beds, Chem. Eng. Sci. 30 (1975) 999–1001.
[39] D.L. Koch, J.F. Brady, Dispersion in fixed beds, J. Fluid Mech. 154 (1985) 399–427.
[40] M.F. Edwards, J.E. Richardson, Gas dispersion in packed beds, Chem. Eng. Sci. 23 (1968) 109–123.
[41] M. Winterberg, E. Tsotsas, Modeling of heat transport in beds packed with spherical particles for various geometries and/or thermal boundary conditions, Int. J. Therm. Sci. 39 (2000) 556–570.
[42] G. Rexwinkel, A.B.M. Heesink, W.P.M. Van Swaaij, Mass transfer in packed beds at low Peclet numbers-wrong experiments or wrong interpretations? Chem. Eng. Sci. 52 (1997) 3995–4003.
[43] J.P. Sorensen, W.E. Stewart, Computation of forced convection in slow flow through ducts and packed beds – III: heat and mass transfer in a simple cubic array of spheres, Chem. Eng. Sci. 29 (1974) 827–832.
[44] D. Kunii, M. Susuki, Particle-to-fluid heat and mass transfer in packed beds of fine particles, Int. J. Heat Mass Transfer 10 (1967) 845–852.
[45] N. Wakao, T. Funazkri, Effect of fluid dispersion coefficients on particle-to-fluid mass transfer coefficients in packed beds, Chem. Eng. Sci. 33 (1978) 1375–1384.
[46] H. Martin, Low Peclet number particle-to-fluid heat and mass transfer in packed beds, Chem. Eng. Sci. 33 (1978) 913–919.
[47] H. Grober, S. Erk, Fundamentals of Heat Transfer, McGraw Hill, New York, 1961.
[48] B.P. Singh, M. Kaviani, Effect of solid conductivity on radiative heat transfer in packed beds, Int. J. Heat Mass Transfer 16 (1994) 2579–2583.
[49] R.H. Perry, D.W. Green, Perry's Chemical Engineers' Hand Book, seventh ed., McGraw Hill, New York, 1997.
[50] E.N. Fuller, P.D. Schettler, J.C. Giddings, Ind. Eng. Chem. 58 (1966) 19–27.
[51] V. Doormal, G.D. Raithby, Enhancements of the SIMPLE method for predicting incompressible fluid flow, Numer. Heat Transfer 7 (1984) 147–163.
[52] J.H. Ferziger, M. Peric, Computational Methods for Fluid Dynamics, second ed., Springer, Berlin, 1999, pp. 74–75.
[53] FLUENT 6.0 UDF Manual, Fluent Inc., New Hampshire, 2001.
[54] D.G. Drake, D.S. Riley, R.R. Baker, K.D. Kilburn, On a Cell to measure diffusion coefficient of gases through cigarette papers, Int. J. Heat Mass transfer 23 (1980) 127–134.
[55] R.R. Baker, D.F. Robinson, Semi-theoretical model for prediction of smoke deliveries, in: Papers Presented at the Joint Meeting of the Smoke and Technology Groups, Harare, Zimbabwe, October 9–14, CORESTA Congress, Paris, 1994, pp. 63–73.
[56] R.R. Baker, R.A. Crellin, The diffusion of carbon monoxide out of cigarettes, Beitr. Tabakforsch. 9 (1977) 131–140.
[57] D. Layten, T. Nielsen, Tobacco Production, Chemistry and Technology, Blackwell Science Ltd., MA, 2002, pp. 418–419.
[58] R.R. Baker, Temperature variation within a cigarette combustion coal during the smoldering cycle, High Temp. Sci. 7 (1975) 236–247.